J Biomol NMR (2015) 62:7–15
DOI 10.1007/s10858-015-9910-2

COMMUNICATION

MAS solid state NMR of proteins: simultaneous ^{15}N–^{13}CA and ^{15}N–^{13}CO dipolar recoupling via low-power symmetry-based RF pulse schemes

Christian Herbst · Peter Bellstedt · Matthias Görlach · Ramadurai Ramachandran

Received: 12 December 2014 / Accepted: 14 February 2015 / Published online: 25 February 2015

Abstract The generation of efficient $RN_n^{\nu}s,^{\nu}k$ symmetry-based low-power RF pulse schemes for simultaneous ^{15}N–^{13}CA and ^{15}N–^{13}CO dipolar recoupling is demonstrated. The method involves mixing schemes employing phase and amplitude-modulated *dual band-selective* 180° pulses as basic "*R*" element and tailoring of the RF field-modulation profile of the 180° pulses so as to obtain efficient magnetisation transfer characteristics over the resonance offset range of the nuclei involved. Mixing schemes leading to simultaneous ^{15}N–^{13}CA and ^{15}N–^{13}CO dipolar recoupling would permit the one-shot acquisition of different chemical shift correlation spectra that are typically utilized for protein backbone resonance assignments and thereby save data acquisition time. At representative MAS frequencies the efficacies of the mixing schemes presented here have been experimentally demonstrated via the simultaneous acquisition of {3D CONH and 3D CANH}, {3D CONH and 3D CO(CA)NH} and {3D CONH, 3D CANH, 3D CO(CA)NH and 3D CA(CO)NH} spectra generated via the magnetisation transfer pathways ^{1}H → ^{13}CO → ^{15}N → ^{1}H (CONH), ^{1}H → ^{13}CA → ^{15}N → ^{1}H (CANH) and ^{1}H → ^{13}CO → ^{13}CA → ^{15}N → ^{1}H (CO(CA)NH) and ^{1}H → ^{13}CA → ^{13}CO → ^{15}N → ^{1}H (CA(CO)NH).

Keywords MAS solids state NMR · Symmetry-based mixing · Protein resonance assignment · Dipolar recoupling · Chemical shift correlation

Introduction

In recent years magic angle spinning solid state NMR spectroscopy (MAS ssNMR) has emerged as a powerful tool in the study of microcrystalline, amyloid and membrane associated proteins. The critical first step in NMR based structural investigations is the assignment of resonances to specific nuclei in the protein. This is typically achieved, irrespective of whether one is dealing with a fully protonated or a perdeuterated protein sample, by carrying out a variety of multi-dimensional chemical shift correlation experiments employing RF pulse schemes with mixing periods leading to dipolar/scalar coupling mediated magnetisation transfers (Pauli et al. 2001; McDermott et al. 2000; Baldus 2002; Baldus et al. 1998; Linser et al. 2008, 2010a, 2010b; Linser 2012; Zhou et al. 2007a; Knight et al. 2011; Marchetti et al. 2012; Zhou et al. 2012; Barbet-Massin et al. 2014; Ward et al. 2011). For example, 3D correlation experiments such as 3D CANH, 3D CA(CO)NH, 3D CONH, 3D CO(CA)NH 3D CBCANH, 3D CBCA(CO)NH and 3D DQ(CACO)NH involving ^{1}H detection have been extensively applied in the literature (Zhou et al. 2007b; Knight et al. 2011; Marchetti et al. 2012; Zhou et al. 2012; Barbet-Massin et al. 2014; Ward et al. 2011). An analysis of such correlation spectra provides information on intra- and inter-residue ^{13}C chemical shifts as basis of sequential resonance assignment. For

Electronic supplementary material The online version of this article (doi:10.1007/s10858-015-9910-2) contains supplementary material, which is available to authorized users.

C. Herbst · P. Bellstedt · M. Görlach · R. Ramachandran (✉)
Research group Biomolecular NMR Spectroscopy, Leibniz Institute for Age Research, Fritz Lipmann Institute, 07745 Jena, Germany
e-mail: raman@fli-leibniz.de

Present Address:
C. Herbst
Department of Physics, Faculty of Science, Ubon Ratchathani University, Ubon Ratchathani 34190, Thailand

example, two adjacent amino acid residues can be linked by matching the ^{13}CO chemical shifts of the correlation peaks seen for the amide groups $(NH)_i$ and $(NH)_{i+1}$ in the 3D CO(CA)NH and 3D CONH spectra, respectively. Alternatively, two adjacent amino acid residues can be linked by matching the ^{13}CA chemical shifts of the correlation peaks seen for the $(NH)_i$ and $(NH)_{i+1}$ amide groups in the 3D CANH and 3D CA(CO)NH spectra, respectively. Typically, the required pairs of experiments, e.g. CONH and CO(CA)NH, are carried out *separately* employing band-selective $^{13}CO \rightarrow {}^{15}N$ and $^{13}CA \rightarrow {}^{15}N$ mixing schemes. However, it is possible to obtain information contained in such experiments in *one-shot*, thereby saving data acquisition time, by employing mixing schemes leading to *simultaneous* $^{13}CO \rightarrow {}^{15}N$ and $^{13}CA \rightarrow {}^{15}N$ magnetisation transfers. For example, in the CO(CA)NH experiment, involving the magnetisation transfer pathway $^{1}H \rightarrow {}^{13}CO_i\ (t_1) \rightarrow {}^{13}CA_i \rightarrow {}^{15}N_i\ (t_2) \rightarrow {}^{1}H_{Ni}(t_3)$, dipolar coupling mediated mixing schemes are typically user for $^{13}CO \rightarrow {}^{13}CA$ magnetisation transfers. Such mixing schemes do not lead to a complete transfer of magnetisation from ^{13}CO to the ^{13}CA nuclei and the ^{13}CO magnetisation remaining after the $^{13}CO \rightarrow {}^{13}CA$ transfer step is typically discarded due to the subsequent application of a band-selective $^{13}CA \rightarrow {}^{15}N$ mixing sequence. However, in situations amenable to employing mixing schemes leading to simultaneous $^{13}CO \rightarrow {}^{15}N$ and $^{13}CA \rightarrow {}^{15}N$ magnetisation transfers, the residual ^{13}CO magnetisation can be effectively used to link the $^{13}CO_i$ to the $(NH)_{i+1}$ amide group. This should lead to a correlation spectrum, arising via the magnetisation transfer pathways $^{1}H \rightarrow {}^{13}CO \rightarrow {}^{13}CA \rightarrow {}^{15}N \rightarrow {}^{1}H$ and $^{1}H \rightarrow {}^{13}CO \rightarrow {}^{13}CO \rightarrow {}^{15}N \rightarrow {}^{1}H$, where every amide group $(NH)_i$ gives rise to two correlation peaks in the ω_1 dimension at the chemical shifts positions of intra- and inter-residue residue $^{13}CO_i$ and $^{13}CO_{i-1}$ nuclei. Thus, the availability of mixing schemes for simultaneous $^{13}CO \rightarrow {}^{15}N$ and $^{13}CA \rightarrow {}^{15}N$ magnetisation transfers would allow to implement efficient RF pulse schemes for achieving sequential resonance assignments for perdeuterated as well as for fully protonated proteins. One approach to achieve simultaneous $^{13}CO \rightarrow {}^{15}N$ and $^{13}CA \rightarrow {}^{15}N$ magnetisation transfers, as shown recently, is via the application of broadband $RN_n^{\nu}s,^{\nu}k$ symmetry-based dual channel RF pulse schemes (Levitt 2007; Brinkmann and Levitt 2001; Herbst et al. 2010; Bellstedt et al. 2012). Our numerical approach to the design of R-symmetry-based γ-encoded ^{15}N–^{13}C dipolar recoupling sequences involves first the identification of appropriate symmetries that would potentially lead to satisfactory solutions at the MAS frequency to be employed and with the available/applicable RF power (Herbst et al. 2010). In the second step, phase/amplitude modulated *broadband* 180° RF pulses with appropriate duration, as determined by the symmetry and MAS frequency, were generated considering a simple spin 1/2 system and different inversion bandwidths. In the final step, these pulses were used as starting basic elements in implementing the symmetry-based pulse schemes. The RF field modulation profiles of the basic elements were then numerically optimised so as to generate RF pulse sequences with satisfactory magnetisation transfer characteristics over the required range of resonance offsets and RF field inhomogeneities. As the ^{13}CO and ^{13}CA nuclei have a chemical shift separation of $\sim$ 120 ppm, broadband ^{13}C–^{15}N dipolar recoupling sequences generally require high ^{13}C RF field strengths. However, we believe that to minimise sample heating effects in temperature sensitive samples it would be advantageous to employ mixing sequences with low RF power requirements. In this context, we have studied the generation of efficient $RN_n^{\nu}s,^{\nu}k$ symmetry-based mixing schemes for simultaneous $^{13}CO \rightarrow {}^{15}N$ and $^{13}CA \rightarrow {}^{15}N$ magnetisation transfer at only low RF power levels. This has been achieved by using phase and amplitude-modulated *dual band-selective,* rather than ^{13}C broadband, 180° pulses as the starting basic "*R*" element in the numerical optimisation procedure. The performance characteristics of the sequences generated were evaluated via numerical simulations and by the acquisition of different chemical shift correlation spectra that are typically employed in protein backbone resonance assignment. The results from these investigations are reported here.

Materials and methods

Multi-dimensional chemical shift correlation experiments were carried out at different MAS frequencies with a Bruker 500 MHz wide-bore Avance III solid state NMR spectrometer equipped with a 2.5 mm triple resonance probe and with the sample temperature kept at $\sim$288 K. Protonated and perdeuterated, uniformly (^{13}C,^{15}N) labelled microcrystalline samples of GB1 and the chicken α-spectrin SH3 domain were prepared as reported in the literature and in our earlier studies (Bellstedt et al. 2012). Chemical shift assignments for the chicken α-spectrin SH3 domain were taken from the literature (Pauli et al. 2001; van Rossum et al. 2003; Lewandowski et al. 2011). For generating $RN_n^{\nu}s,^{\nu}k$ symmetry-based ^{15}N–^{13}C mixing sequences leading to γ-encoded heteronuclear double-quantum dipolar recoupling, with suppression of chemical shift anisotropies and homonuclear dipolar coupling terms (Brinkmann and Levitt 2001), ^{13}C/^{15}N RF field strengths and MAS frequencies in the range of 20–30 kHz and 15–33 kHz, respectively, have been considered. Calculations were carried out with typical CSA parameters (Herbst et al. 2010) in the ^{15}N and ^{13}C channel. Phase and

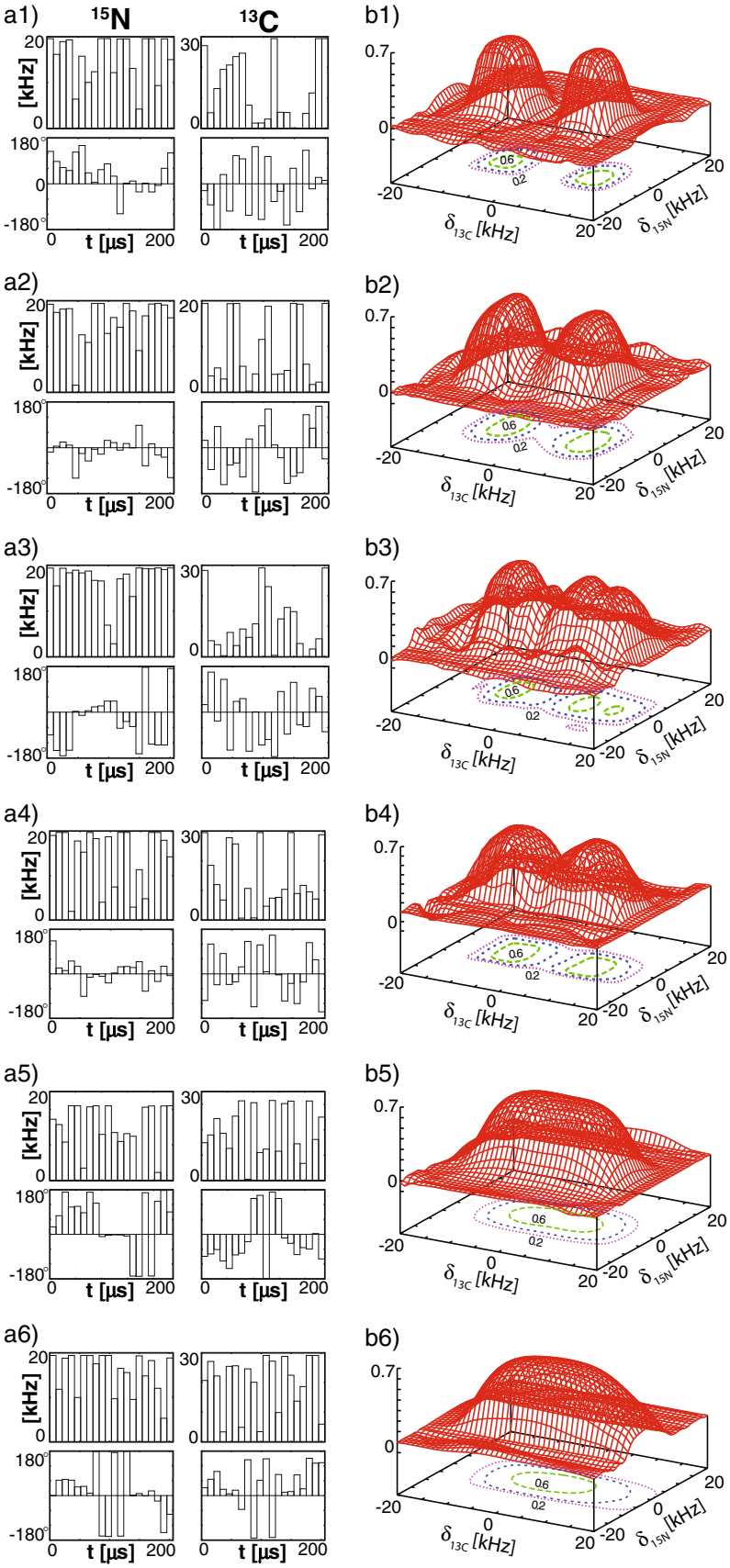

Fig. 1 Amplitude and phase-modulation profiles (**a**1–6) and simulated $^{13}C \rightarrow {}^{15}N$ magnetisation transfer characteristics (**b**1–6) of the numerically optimised symmetries $R16_{49}^{-5,4}$ (**a**1; 15 kHz MAS; 600 MHz), $R16_{66}^{-5,3}$(**a**2; 20 kHz MAS; 500 MHz), $R16_{66}^{-5,3}$(**a**3; 20 kHz MAS; 500 MHz), $R16_{65}^{-4,3}$(**a**4; 20 kHz MAS; 500 MHz), $R14_{111}^{-3,4}$ (**a**5; 33.333 kHz MAS; 500 MHz) and $R16_{110}^{-3,5}$ (**a**6; 33.333 kHz MAS; 500 MHz). The optimised amplitude and phase-modulation profiles were generated for a resonance offset range of ±2 kHz and maximum ^{13}C and ^{15}N RF field strengths shown. Plots given in (**b**1–6) show the magnitude of the transferred magnetisation on nitrogen at a τ_{mix} of ~3.3 ms as a function of the resonance offsets of the dipolar coupled nuclei, starting with z magnetisation on the carbon (^{13}C) spin at zero mixing time. The simulations were carried out using appropriate chemical shift, scalar and dipolar coupling parameters (Herbst et al. 2010). The RF amplitude and phase values of the slices of the basic R elements are given in the supplementary material (Table S1)

amplitude modulated dual band-selective 180° pulses, implemented as a sandwich of a small number of pulses of equal duration and generated via the global optimisation procedure "genetic algorithms" (GA) were employed as the starting basic "*R*" element (supplementary material, Figs. S1–S2). The phase and amplitude modulation profiles were subsequently tailored numerically via the nonlinear least-squares optimisation procedure NL2SOL implemented in SPINEVOLUTION (Veshtort and Griffin 2006) to achieve satisfactory performance of the mixing sequence over the required resonance offset range of the nuclei. Selected symmetries for which the starting basic elements of the required duration could be constructed were considered in the numerical design. In order to find the best possible solution, the optimisation calculations were started with a variety of basic elements corresponding to RF pulses with different inversion bandwidths and phase and amplitude modulation profile characteristics. Unless stated otherwise, numerical calculations were restricted to a Zeeman field strength equivalent to a ^{1}H resonance frequency of 500 MHz and were carried out with a two spin ^{15}N–^{13}C system using standard dipolar coupling and chemical shift parameters. Optimised RF pulse schemes considering a mixing time of ~3 ms were generated by maximising the transfer of longitudinal magnetisation to the second spin (^{13}C), starting with a z magnetisation on spin 1 (^{15}N) at zero mixing time. In general, the local optimisation calculations were repeated several times varying all the RF phase and amplitude values randomly over a range of ±10 %. Numerical calculations were carried on a UNIX cluster with 64 processors, incorporating RF field inhomogeneities (±5 %) and allowing only a limited number of 32 crystallite orientations selected according to the Zaremba–Cheng–Wolfsberg (ZCW) method (Cheng et al. 1973). All simulations to assess the performance characteristics of the pulse sequences were carried out with SPINEVOLUTION (Veshtort and Griffin 2006) considering 168 α and β powder angles selected according to the REPULSION scheme (Bak and Nielsen 1997) and 16 γ angles. Other details are given in the figure captions. Unless indicated otherwise, all spectra were collected with simultaneous ^{1}H decoupling during ^{15}N–^{13}C mixing. Phase sensitive chemical shift correlation spectra were generated by the States procedure (States et al. 1982). Standard phase cycling was employed to select signals arising from desired coherence transfer pathways.

Results and discussion

Numerical optimisation runs for generating dipolar recoupling schemes to achieve simultaneous ^{13}CO → ^{15}N and ^{13}CA → ^{15}N magnetisation transfers were carried out at MAS frequencies of 15, 20 and 33.333 kHz considering representative values for the range of resonance offsets and RF field strengths. The simulated performance characteristics of selected mixing sequences are shown in Fig. 1 along with the optimised RF field-modulation profiles of the basic elements (Fig. 1a1–6). The optimised profiles were obtained without imposing any restriction on the phase and amplitude modulation profile characteristics and typically using a resonance offset range of (±2 kHz, ±2 kHz) for the ^{13}C and ^{15}N nuclei and RF field strengths indicated. The plots (Fig. 1b1–6) show the magnitude of the simulated transferred magnetisation (normalised to the maximum transferable signal) on nitrogen at τ_{mix} of ~3.3 ms, starting with z magnetisation on carbon at zero mixing time and keeping the ^{13}C RF carrier at the middle of the spectral range. The performance of the numerically optimised symmetry-based schemes reported here were generally found to be not affected by minor variations (±5 %) in the RF field strength. From the numerical simulation results (Fig. 1) it becomes obvious, that by choosing appropriate symmetries efficient ^{13}C–^{15}N dipolar recoupling schemes for simultaneous ^{13}CO → ^{15}N and ^{13}CA → ^{15}N magnetisation transfers can be implemented—even for high MAS frequencies and using only

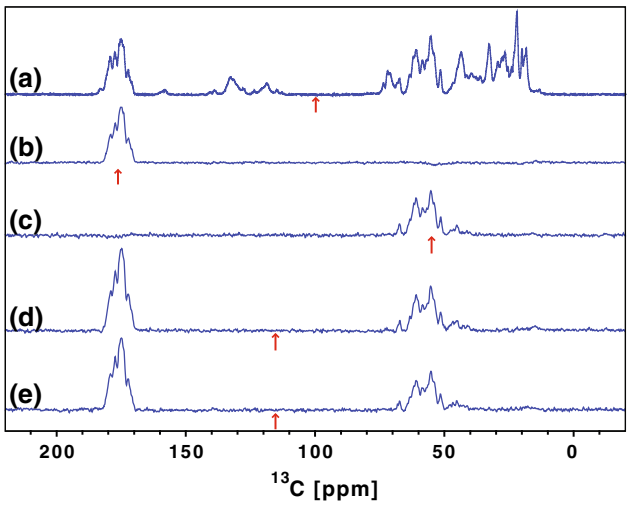

Fig. 2 1D ^{13}C NMR spectra of GB1 recorded at a spinning rate of 20 kHz following a simple ^{1}H → ^{13}C CP *a*, ^{1}H → ^{15}N CP followed by ^{15}N → ^{13}C band-selective *b*, *c* and dual band-selective *d*, *e* mixing schemes, respectively. The ^{13}C RF carrier positions are indicated. Spectra *b*–*c*) were recorded with the $R16_{49}^{-5,4}$ symmetry-based mixing scheme (Herbst et al. 2011) using ^{13}C and ^{15}N RF field strengths of 13.3 kHz. Spectra *d* and *e* were recorded with $R16_{66}^{-5,3}$ and $R16_{65}^{-4,3}$ symmetry-based mixing schemes, respectively, with the following parameters: ^{15}N RF field strengths of 20 kHz, a ^{13}C RF field strengths of 20 kHz *d* and 30 kHz *e*, 256 scans, 2 s recycle time, ^{1}H–^{13}C CP contact time of 1 ms (*a*), ^{1}H–^{15}N CP contact time of 0.9 ms (*b*–*e*), ^{15}N–^{13}C mixing times of 2.45 ms (*b*,*c*), 3.3 ms (*d*) and 3.25 ms (*e*). Spectra *b*–*e* were recorded under ^{1}H decoupling during ^{15}N–^{13}C mixing

moderate $^{13}C/^{15}N$ RF field strengths. The mixing sequences reported here were generated without imposing any restriction for minimising the transfer outside the $^{15}N/^{13}C$ spectral windows of interest. Although the mixing sequences were designed for a particular MAS frequency, by appropriate scaling of the duration of the optimised basic element and RF field strength, satisfactory magnetisation transfer characteristics (over the correspondingly scaled spectral range) at other MAS frequencies can be realised.

The performance characteristics of the symmetry-based sequences were validated via experimental measurements and representative data are presented here. One-dimensional ^{13}C spectra of the GB1 sample were collected at a spinning rate of 20 kHz via direct CP from ^{1}H to all ^{13}C nuclei (Fig. 2a), direct CP from ^{1}H to ^{15}N followed by band selective ^{15}N–^{13}C mixing using the mixing sequence $R16_{49}^{-5,4}$ (Herbst et al. 2011), keeping the ^{13}C carrier at 175 (Fig. 2b) and 55 ppm (Fig. 2c), respectively. In addition, direct CP from ^{1}H to ^{15}N followed by simultaneous $^{15}N \rightarrow {}^{13}CA$ and $^{15}N \rightarrow {}^{13}CO$ transfers via the mixing sequences $R16_{66}^{-5,3}$ (Fig. 2d) and $R16_{65}^{-4,3}$ (Fig. 2e) reported here was carried out keeping the ^{13}C RF carrier at 115 ppm. As already emphasised, the sequences reported here can also be applied at other frequencies by appropriate scaling of the RF field strength and duration of the respective basic elements. An example of this scalability is demonstrated in Fig. 3 that shows the 2D ^{15}N–^{13}C correlation spectrum of GB1 recorded at 500 MHz and at a spinning frequency of 12.5 kHz generated using the dual band-selective $R16_{49}^{-5,4}$ symmetry scheme. The ^{15}N–^{13}CA and ^{15}N–^{13}CO correlation peak patterns essentially matches with that obtained via band-selective mixing sequences and the 1D and 2D spectra clearly demonstrate that simultaneous ^{15}N–^{13}CA and ^{15}N–^{13}CO dipolar recoupling via symmetry-based sequences can be achieved employing low RF field strengths. The potential of such mixing sequences in protein sequential resonance assignment has been examined using the RF pulse schemes given in Fig. 4.

The scheme in Fig. 4a is essentially similar to that employed for generating 3D CNH correlation data via the magnetisation transfer pathway $^{1}H \rightarrow {}^{13}CA/{}^{13}CO \rightarrow {}^{15}N \rightarrow {}^{1}H$ except that it involves an additional ^{13}C–^{13}C mixing step preceding the ^{13}C–^{15}N mixing period. The initial transverse ^{13}C magnetisation is first generated by a

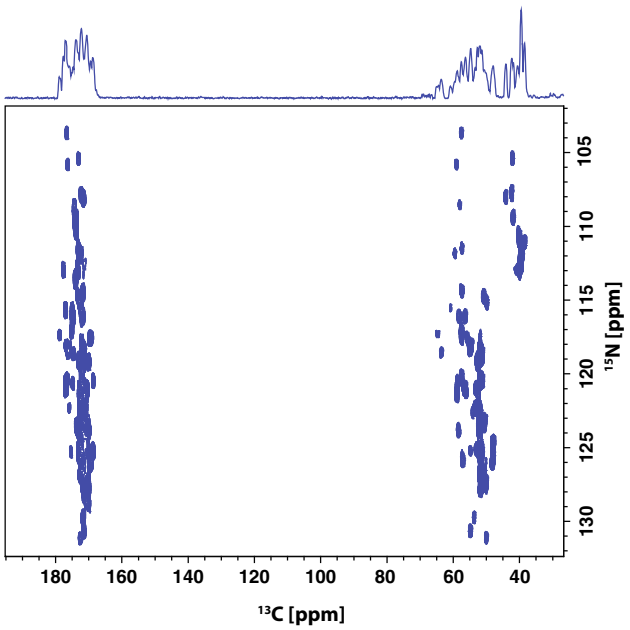

Fig. 3 2D ^{15}N–^{13}C chemical shift correlation spectrum of perdeuterated GB1 (*crystal* form A) recorded at 500 MHz and a spinning rate of 12.5 kHz with ^{1}H decoupling during mixing. The dual band-selective $R16_{49}^{-5,4}$ symmetry scheme with the corresponding *scaled* numerically optimised *R* element given in Fig. 1a, CP contact time of 1 ms, ^{15}N–^{13}C mixing time (τ_{mix}) of 3.92 ms, ^{13}C and ^{15}N mixing RF field strengths of 24 and 16 kHz, respectively, 512 transients per t_1 increment, 60 t_1 increments, spectral width in the indirect dimension of 2000 Hz and a recycle time of 2 s were used, keeping the ^{13}C and ^{15}N RF carriers at 115 and 118 ppm, respectively

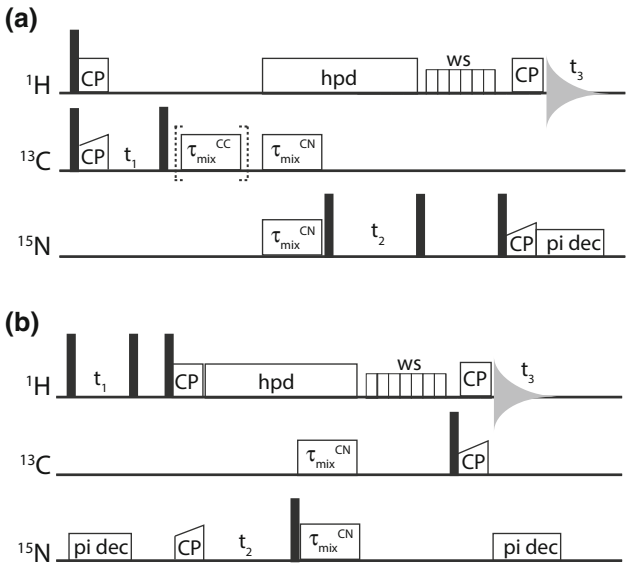

Fig. 4 RF pulse schemes employed for the acquisition of 3D C(C)NH (**a**) and 3D HN(C)H (**b**) correlation spectra. Filled rectangles represent 90° pulses. The $^{1}H \rightarrow {}^{13}C$ CP in pulse scheme **a** was carried out using low or high RF power levels to achieve either band-selective transfer of polarisation to ^{13}CO or simultaneous transfers to ^{13}CO and ^{13}CA, respectively. Dipolar or scalar coupling mediated mixing schemes were employed to achieve ^{13}C–^{13}C mixing. 3D CNH correlation spectra were generated omitting the ^{13}C–^{13}C mixing period. ^{13}C–> ^{1}H reverse CP in scheme **b** was applied to achieve polarisation transfers from both the ^{13}CO and ^{13}CA nuclei. For water suppression (WS), proton saturation pulses with alternating *x* and *y* phases (Zhou and Rienstra 2008) were applied for ~100–200 ms at a power level of 25 kHz. The ^{13}C RF carrier was kept at 115 ppm during the ^{13}C–^{13}C and ^{13}C–^{15}N mixing periods

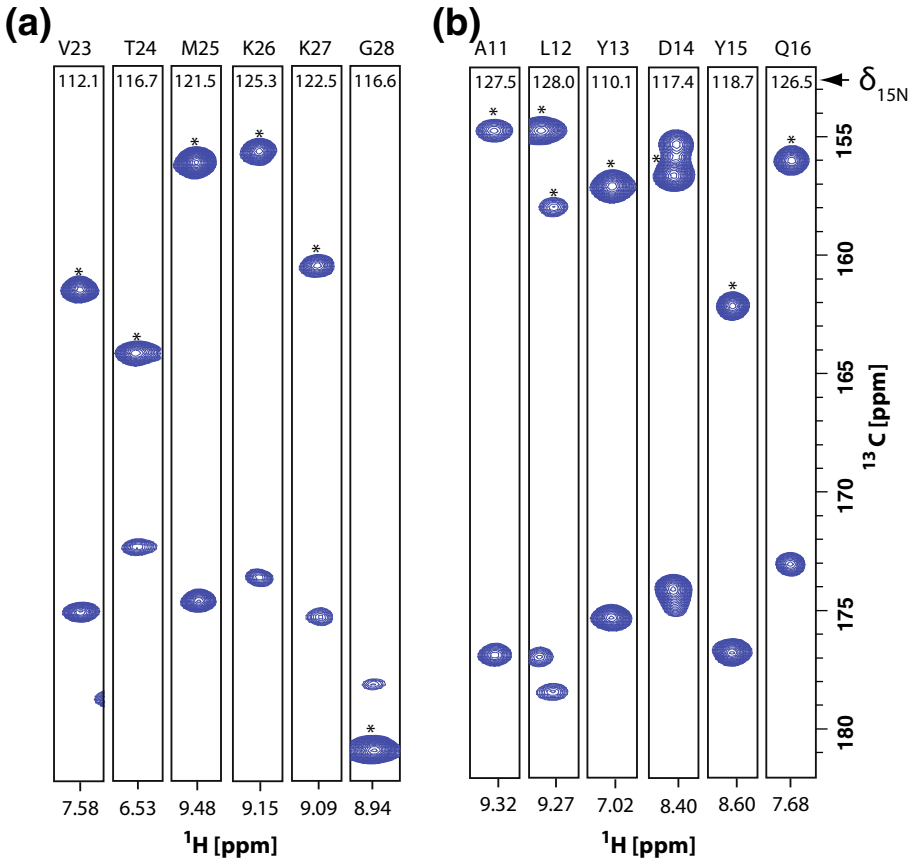

Fig. 5 Spectral cross-sections taken from the 3D CNH chemical shift correlation spectra of perdeuterated SH3 domain of chicken α-spectrin (NH:ND 30:70), resulting from the magnetisation transfer pathway $^{1}H \rightarrow {}^{13}C \rightarrow {}^{15}N \rightarrow {}^{1}H$, and recorded at 500 MHz and spinning frequency of 20 kHz (**a**), and 33.333 kHz (**b**), respectively. The symmetries $R16_{66}^{-5,3}$ (**a**), and $R14_{111}^{-3,4}$ (**b**), with the corresponding numerically optimised *R* elements (Fig. 1), $^{1}H–^{13}C$ CP contact time of 3 ms (**a**) and 2.5 ms (**b**), $^{1}H–^{15}N$ CP contact time of 0.3 ms (**a**) and 0.5 ms (**b**), $^{15}N–^{13}C$ mixing time of 3.3 ms (**a**) and 3.33 ms (**b**), RF field strengths of [20 kHz (^{13}C), 20 kHz (^{15}N)] (**a**) and [30 kHz (^{13}C), 20 kHz (^{15}N)] (**b**) during mixing, 32 transients per t_1 increment, 42 t_1 increments, 24 t_2 increments, spectral widths in the indirect dimensions of 1418 Hz (^{15}N) and 4274 Hz (^{13}C) and a recycle time of 1.0 s were employed. The ^{1}H, ^{15}N and ^{13}C RF carriers were set at 5, 122 and 169 ppm, respectively. The ^{13}C RF carrier was switched to 115 ppm during $^{15}N–^{13}C$ mixing in the presence of ^{1}H decoupling. ^{15}N decoupling in the direct dimension was carried out via the repetitive application of ^{15}N π pulses (Zhou et al. 2007a) of 64 μs duration with an inter-pulse delay of 50 μs. The folded ^{13}CA peaks are indicated with an *asterisk*

combination of direct excitation and a cross-polarisation (band-selective or broadband) step (Linser 2012). It then evolves in the absence of ^{1}H decoupling during the t_1 period. The magnetisation at the end of t_1 is flipped to the *z* axis and subjected to a period of $^{13}C \rightarrow {}^{15}N$ longitudinal magnetisation exchange via the application of the mixing sequence leading to simultaneous $^{13}CA \rightarrow {}^{15}N$ and $^{13}CO \rightarrow {}^{15}N$ transfers. Depending on the type of data to be collected, the $^{13}C \rightarrow {}^{15}N$ mixing step is carried out with or without a preceding $^{13}C–^{13}C$ dipolar/scalar coupling mediated mixing sequence resulting in a longitudinal magnetisation exchange. The ^{15}N polarisation generated at the end of the heteronuclear mixing period is brought to the transverse plane and evolves during the t_2 period. The magnetisation at the end of the t_2 is then flipped to the *z* axis. Proton saturation pulses with alternating *x* and *y* phases were then applied for 100–200 ms at a power level of ~25 kHz to achieve water suppression (Zhou and Rienstra 2008). Subsequently, the ^{15}N longitudinal magnetisation is brought to the transverse plane and subjected to a CP step for transferring the magnetisation to the directly attached proton and for direct detection in t_3. The ^{13}C RF carrier was kept near the CO region during the t_1 period and the spectral width was adjusted so as to fold the ^{13}CA resonances into the ^{13}CO spectral window. Using mixing sequences leading to simultaneous $^{13}CA \rightarrow {}^{15}N$ and $^{13}CO \rightarrow {}^{15}N$ transfers, the RF pulse scheme was successfully employed to generate different 3D correlation spectra of the perdeuterated chicken α-spectrin SH3 domain. The spectral cross-sections taken from the 3D CNH correlation spectra (Fig. 5) demonstrate the satisfactory performance of the $^{13}C \rightarrow {}^{15}N$ mixing sequences for one-shot collection of 3D CONH and 3D CANH correlation

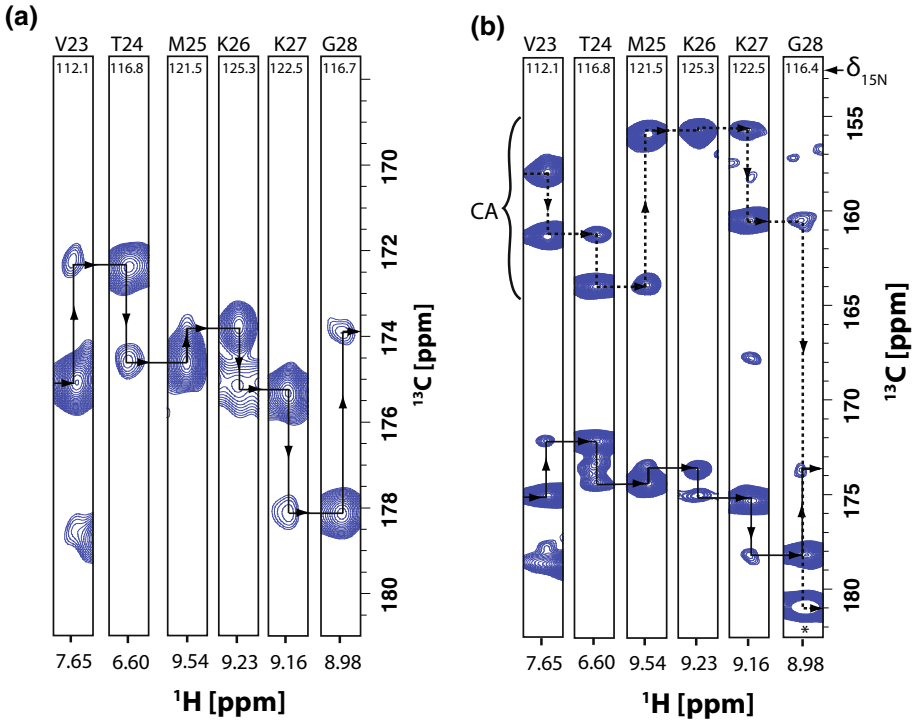

Fig. 6 ^{13}CO–^{1}H spectral cross-sections of 3D CO(CA)NH (**a**) and 3D C(C)NH (**b**) spectra of perdeuterated SH3 domain of chicken α-spectrin (NH:ND 30:70) recorded at 500 MHz and a spinning rate of 20 kHz. The ^{15}N chemical shift positions at which the cross-sections were taken are indicated and show the sequential walk along the backbone residues V23–G28. The 3D spectra were recorded starting with band-selective transfer of ^{1}H polarisation to ^{13}CO (**a**) and with simultaneous transfers to ^{13}CO and ^{13}CA (**b**), respectively. RFDR with tanh/tan adiabatic inversion pulses (Leppert et al. 2003) was employed for ^{13}CO–^{13}CA dipolar mixing (τ_{mix} = 1.8 ms). The $R16_{66}^{-5,3}$ symmetry was used for dual band-selective ^{15}N–^{13}C mixing. Spectra were recorded with a ^{1}H–^{13}C CP contact time of 3 ms, ^{1}H–^{15}N CP contact time of 0.3 ms, ^{15}N–^{13}C mixing time of 3.3 ms, ^{13}C and ^{15}N RF field strength of 20 kHz during mixing, 64 (**a**) and 48 (**b**) transients per t_1 increment, 25 (**a**) and 48 (**b**) t_1 increments, 32 t_2 increments, spectral widths in the indirect dimensions of 1418 Hz (^{15}N) and (1885 Hz (**a**) or 4274 Hz (**b**)) (^{13}C) and a recycle time of 1.0 s. The ^{1}H, ^{15}N and ^{13}C RF carriers were set to 5, 122 and (175 ppm (a) and 169 ppm (b)), respectively. The ^{13}C RF carrier was switched to 115 ppm during ^{13}CO–^{13}CA and ^{15}N–^{13}C mixing in both cases. Folded ^{13}CA *peaks* are indicated

spectra. The data has been generated employing a broadband ^{1}H → ^{13}C CP step and without a ^{13}C–^{13}C mixing step preceding the ^{13}C–^{15}N mixing period. Cross-sections of 3D CO(CA)NH and CO/CA(C)NH correlation spectra using a band-selective (Fig. 6a) or broadband ^{1}H → ^{13}C CP step (Fig. 6b) demonstrate the utility of mixing sequences leading to simultaneous ^{13}CA → ^{15}N and ^{13}CO → ^{15}N magnetisation transfers for achieving protein sequential backbone resonance assignment. Both data sets were generated with a ^{13}C–^{13}C dipolar mixing step preceding the ^{13}C–^{15}N mixing period and at a MAS frequency of 20 kHz. The cross-peaks appearing in the correlation spectrum (Fig. 6a) arise via the magnetisation transfer pathways ^{1}H → ^{13}CO → ^{13}CA → ^{15}N → ^{1}H and ^{1}H → ^{13}CO → ^{13}CO → ^{15}N → ^{1}H. On the other hand, Fig. 6b demonstrates the simultaneous collection of data arising via four different magnetisation transfer pathways: ^{1}H → ^{13}CO → ^{13}CA → ^{15}N → ^{1}H, ^{1}H → ^{13}CO → ^{13}CO → ^{15}N → ^{1}H, ^{1}H → ^{13}CA → ^{13}CO → ^{15}N → ^{1}H and ^{1}H → ^{13}CA → ^{13}CA → ^{15}N → ^{1}H. In addition to ^{13}C–^{13}C dipolar mixing sequences, 3D correlation spectra such as CO(CA)NH and C(C)NH can also be generated with scalar coupling mediated mixing schemes employing appropriate mixing periods. An example of a 3D C(C)NH correlation spectrum of the SH3 domain recorded with a low-power TOBSY mixing sequence at a spinning speed of 33.333 kHz is given in the supplementary material (Fig. S3) along with the spectral cross-sections depicting the sequential walk along the backbone residues spanning the region V23–G28. It is worth noting that by simultaneous ^{13}CO → ^{15}N and ^{13}CA → ^{15}N magnetisation transfer, two adjacent amino acid residues can be linked by matching the ^{13}CO chemical shifts of the correlation peaks seen for the amide groups $(NH)_i$ and $(NH)_{i+1}$ in the 3D CO(CA)NH. On the other hand, both the ^{13}CO as well as ^{13}CA chemical shifts can be utilised for unambiguous linking of two adjacent amino acid residues via the 3D C(C)NH experiment.

In addition to 3D CNH, 3D CO(CA)NH and 3D C(C)NH experiments, mixing schemes leading to simultaneous ^{13}CO → ^{15}N and ^{13}CA → ^{15}N transfers can also

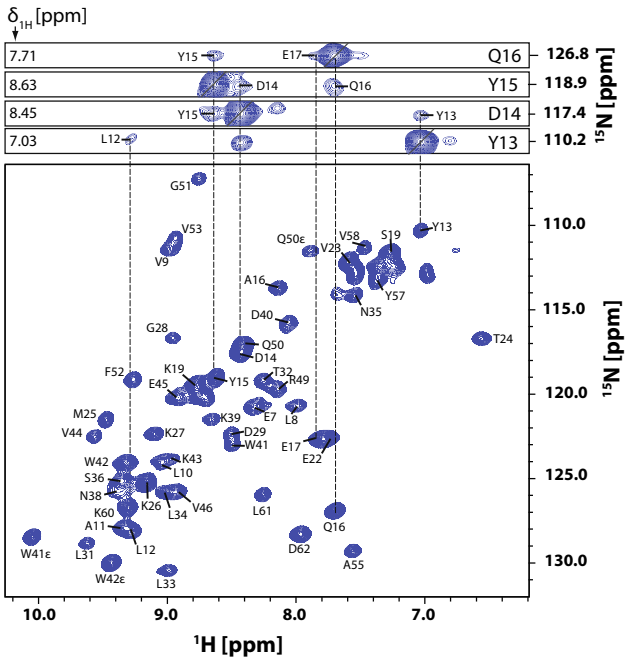

Fig. 7 Representative spectral cross-sections (ω_{13}) taken from the 3D HN(C)H chemical shift correlation spectrum of perdeuterated SH3 domain of chicken α-spectrin (NH:ND 30:70) recorded at 500 MHz and a spinning rate of 33.333 kHz. The 3D spectrum was recorded using the $R14_{111}^{-3,4}$ symmetry-based ^{15}N–^{13}C mixing, a ^{1}H–^{15}N CP contact time of 0.5 ms, ^{1}H–^{13}C CP contact time of 4 ms, ^{15}N–^{13}C mixing time of 3.33 ms, ^{13}C and ^{15}N RF field strengths of 30 and 20 kHz, respectively, during mixing, 64 transients per t_1 increment, 38 t_1 increments, 23 t_2 increments, spectral widths in the indirect dimensions of 1418 Hz (^{15}N) and 2249 Hz (^{1}H) and a recycle time of 1.0 s. The ^{1}H, ^{15}N and ^{13}C RF carriers were set to 8.5, 122 and 115 ppm, respectively. The ^{15}N–^{1}H (ω_{23}) spectral cross-sections taken at the ^{1}H chemical shift positions indicated show connectivities observed between adjacent residues. The ^{15}N–^{1}H correlation spectrum recorded at a MAS frequency of 33.333 kHz is shown for reference

be effectively applied in acquiring a variety of other chemical shift correlation spectra of interest in MAS ssNMR studies of proteins, e.g. 3D C^{s}(C)NH and 3D HN(C)H. The 3D C^{s}(C)NH chemical shift correlation experiment involving the magnetisation transfer pathway $^{1}H \rightarrow {}^{13}C^{s} \rightarrow (^{13}CA,^{13}CO) \rightarrow {}^{15}N \rightarrow {}^{1}H$ was carried out with a perdeuterated SH3 domain sample at a spinning speed of 33.333 kHz employing a band-selective transfer of ^{1}H polarisation to side chain ^{13}C nuclei, RFDR for ^{13}C–^{13}C dipolar mixing and $R14_{111}^{-3,4}$ symmetry-based ^{15}N–^{13}C mixing. The spectrum obtained (Supplementary material, Fig. S4) suggests that the application of efficient ^{15}N–^{13}C mixing sequences for simultaneous $^{13}CO \rightarrow {}^{15}N$ and $^{13}CA \rightarrow {}^{15}N$ transfers in a 3D C^{s}(C)NH experiment allows, signal to noise ratio permitting, sequential linking of two adjacent amino acid residues via the side chain ^{13}C chemical shifts associated with the amide $(NH)_i$ and $(NH)_{i+1}$correlation peaks. Figure 7 shows data from the 3D HN(C)H chemical shift correlation spectrum of the perdeuterated SH3 domain sample recorded at a spinning speed of 33.333 kHz and arising via the magnetisation transfer pathway $^{1}H_N$ (t_1) → ^{15}N (t_2) → (^{13}CA,^{13}CO) → $^{1}H_N$ (t_3). The experiment was carried out via the RF pulse scheme given in Fig. 4b using the $R14_{111}^{-3,4}$ symmetry-based ^{15}N–^{13}C mixing scheme for simultaneous transfer of the ^{15}N polarisation at the end of the t_2 evolution period to the directly bonded ^{13}CA and ^{13}CO nuclei. In the 3D HN(C)H experiment, the initial $^{1}H_i$ magnetisation is transferred simultaneously via four different pathways: $^{1}H_i \rightarrow {}^{15}N_i \rightarrow {}^{13}CO_{i-1} \rightarrow {}^{1}H_i$, $^{1}H_i \rightarrow {}^{15}N_i \rightarrow {}^{13}CO_{i-1} \rightarrow {}^{1}H_{i-1}$, $^{1}H_i \rightarrow {}^{15}N_i \rightarrow {}^{13}CA_i \rightarrow {}^{1}H_i$ and $^{1}H_i \rightarrow {}^{15}N_i \rightarrow {}^{13}CA_i \rightarrow {}^{1}H_{i+1}$. This results in three correlation peaks at the chemical shift positions ($^{15}N_i$,$^{1}H_i$), ($^{15}N_i$,$^{1}H_{i+1}$) and ($^{15}N_i$, $^{1}H_{i-1}$) in the ω_{23} strips taken at the $^{1}H_i$ chemical shift position in the ω_1 dimension and permit the sequential linking of three adjacent amino acid residues as shown in Fig. 7. The cross-peak patterns observed in the ω_{23} strips are consistent with the assignments reported in the literature.

In conclusion, the results presented here clearly show that mixing schemes leading to simultaneous $^{13}CO \rightarrow {}^{15}N$ and $^{13}CA \rightarrow {}^{15}N$ magnetisation transfers have considerable potential for MAS solid state NMR studies of proteins. It is worth pointing out that the symmetry-based approach is not the only method available to achieve low-power simultaneous N–CO and N–CA dipolar recoupling. A dual band-selective double CP using sinusoidal modulation of the ^{13}C RF amplitude has also been shown recently to be effective for this (Zhang et al. 2012). However, this has been demonstrated only at a moderate MAS frequency of 11 kHz. As demonstrated here, the symmetry-based approach can be exploited to implement low-power mixing sequences for simultaneous recoupling of N–CO and N–CA dipolar interactions even at high MAS frequencies. Although only a few representative implementations of this approach are presented here, mixing schemes leading to simultaneous $^{13}CO \rightarrow {}^{15}N$ and $^{13}CA \rightarrow {}^{15}N$ magnetisation transfers can also be effectively used in a variety of other applications, e.g. in the acquisition of 3D DQ(CACO)NH type of correlation spectra (Ward et al. 2011) or in the simultaneous acquisition of 3D NCACX and 3D NCOCX correlation spectra involving ^{13}C direct detection. We believe that the design and implementation of such mixing schemes will be especially useful at high Zeeman field strengths, as the implementation of *broadband* ^{13}C–^{15}N dipolar recoupling sequences at low power levels will become more difficult due to the large chemical shift separation of the ^{13}CO and ^{13}CA nuclei.

Acknowledgements The FLI is a member of the Science Association'Gottfried Wilhelm Leibniz' (WGL) and is financially supported by the Federal Government of Germany and the State of Thuringia.

References

Bak M, Nielsen NC (1997) REPULSION, a novel approach to efficient powder averaging in solid-state NMR. J Magn Reson 125(1):132–139

Baldus M (2002) Correlation experiments for assignment and structure elucidation of immobilized polypeptides under magic angle spinning. Prog Nucl Magn Reson Spectrosc 41(1–2):1–47

Baldus M, Aneta TP, Herzfeld J, Robert GG (1998) Cross polarization in the tilted frame: assignment and spectral simplification in heteronuclear spin systems. Mol Phys 95(6):1197–1207 Taylor and Francis

Barbet-Massin E, Pell AJ, Retel JS, Andreas LB, Jaudzems K, Franks WT et al (2014) Rapid proton-detected NMR assignment for proteins with fast magic angle spinning. J Am Chem Soc 136(35): 12489–12497

Bellstedt P, Herbst C, Häfner S, Leppert J, Görlach M, Ramachandran R (2012) Solid state NMR of proteins at high MAS frequencies: symmetry-based mixing and simultaneous acquisition of chemical shift correlation spectra. J Biomol NMR 54(4):325–335

Brinkmann A, Levitt MH (2001) Symmetry principles in the nuclear magnetic resonance of spinning solids: heteronuclear recoupling by generalized Hartmann-Hahn sequences. J Chem Phys 115(1): 357–384 AIP Publishing

Cheng VB, Suzukawa HH, Wolfsberg M (1973) Investigations of a nonrandom numerical method for multidimensional integration. J Chem Phys 59(8):3992–3999 AIP Publishing

Herbst C, Herbst J, Carella M, Leppert J, Ohlenschläger O, Görlach M et al (2010) Broadband ^{15}N–^{13}C dipolar recoupling via symmetry-based RF pulse schemes at high MAS frequencies. J Biomol NMR 47(1):7–17

Herbst C, Herbst J, Leppert J, Ohlenschläger O, Görlach M, Ramachandran R (2011) Chemical shift correlation at high MAS frequencies employing low-power symmetry-based mixing schemes. J Biomol NMR 50(3):277–284

Knight MJ, Webber AL, Pell AJ, Guerry P, Barbet-Massin E, Bertini I et al (2011) Fast resonance assignment and fold determination of human superoxide dismutase by high-resolution proton-detected solid-state MAS NMR spectroscopy. Angew Chem Int Ed 50(49):11697–11701

Leppert J, Heise B, Ohlenschläger O, Görlach M, Ramachandran R (2003) Broadband RFDR with adiabatic inversion pulses. J Biomol NMR 26(1):13–24

Levitt MH (2007) Symmetry-based pulse sequences in magic-angle spinning solid-state NMR. eMagRes. Wiley, Chichester

Lewandowski JR, Dumez J-N, Akbey U, Lange S, Emsley L, Oschkinat H (2011) Enhanced resolution and coherence lifetimes in the solid-state NMR spectroscopy of perdeuterated proteins under ultrafast magic-angle spinning. J Phys Chem Lett 2(17): 2205–2211

Linser R (2012) Backbone assignment of perdeuterated proteins using long-range H/C-dipolar transfers. J Biomol NMR 52(2):151–158

Linser R, Fink U, Reif B (2008) Proton-detected scalar coupling based assignment strategies in MAS solid-state NMR spectroscopy applied to perdeuterated proteins. J Magn Reson 193(1): 89–93

Linser R, Fink U, Reif B (2010a) Assignment of dynamic regions in biological solids enabled by spin-state selective NMR experiments. J Am Chem Soc 132(26):8891–8893

Linser R, Fink U, Reif B (2010b) Narrow carbonyl resonances in proton-diluted proteins facilitate NMR assignments in the solid-state. J Biomol NMR 47(1):1–6

Marchetti A, Jehle S, Felletti M, Knight MJ, Wang Y, Xu Z-Q et al (2012) Backbone assignment of fully protonated solid proteins by 1H detection and ultrafast magic-angle-spinning NMR spectroscopy. Angew Chem Int Ed 51(43):10756–10759

McDermott A, Polenova T, Böckmann A, Zilm KW, Paulson EK, Martin RW et al (2000) Partial NMR assignments for uniformly (13C, 15 N)-enriched BPTI in the solid state. J Biomol NMR 16(3):209–219

Pauli J, Baldus M, van Rossum B, de Groot H, Oschkinat H (2001) Backbone and side-chain13c and15 N signal assignments of the α-spectrin SH3 domain by magic angle spinning solid-state NMR at 17.6 Tesla. ChemBioChem 2(4):272–281

States DJ, Haberkorn RA, Ruben DJ (1982) A two-dimensional nuclear overhauser experiment with pure absorption phase in four quadrants. J Magn Reson 48(2):286–292

van Rossum B-J, Castellani F, Pauli J, Rehbein K, Hollander J, de Groot HJM et al (2003) Assignment of amide proton signals by combined evaluation of HN, NN and HNCA MAS-NMR correlation spectra. J Biomol NMR 25(3):217–223

Veshtort M, Griffin RG (2006) SPINEVOLUTION: a powerful tool for the simulation of solid and liquid state NMR experiments. J Magn Reson 178(2):248–282

Ward ME, Shi L, Lake E, Krishnamurthy S, Hutchins H, Brown LS et al (2011) Proton-detected solid-state NMR reveals intramembrane polar networks in a seven-helical transmembrane protein proteorhodopsin. J Am Chem Soc 133(43):17434–17443

Zhang ZZ, Miao YY, Liu XX, Yang JJ, Li CC, Deng FF et al (2012) Dual-band selective double cross polarization for heteronuclear polarization transfer between dilute spins in solid-state MAS NMR. J Magn Reson 31(217):92–99

Zhou DH, Rienstra CM (2008) High-performance solvent suppression for proton detected solid-state NMR. J Magn Reson 192(1): 167–172

Zhou DH, Shea JJ, Nieuwkoop AJ, Franks WT, Wylie BJ, Mullen C et al (2007a) Solid-state protein-structure determination with proton-detected triple-resonance 3D magic-angle-spinning NMR spectroscopy. Angew Chem Int Ed 46(44):8380–8383. doi:10.1002/ange.200702905/full

Zhou DH, Shah G, Cormos M, Mullen C, Sandoz D, Rienstra CM (2007b) Proton-detected solid-state NMR spectroscopy of fully protonated proteins at 40 kHz magic-angle spinning. J Am Chem Soc 129(38):11791–11801

Zhou DH, Nieuwkoop AJ, Berthold DA, Comellas G, Sperling LJ, Tang M et al (2012) Solid-state NMR analysis of membrane proteins and protein aggregates by proton detected spectroscopy. J Biomol NMR 54(3):291–305